Photo-Oxidizing Ruthenium(II) Complexes with Enhanced Visible-Light Absorption and G-quadruplex DNA Binding Abilities

Martin Gillard, Guillaume Piraux, Martin Daenen, Michaël Abraham, Ludovic Troian-Gautier, Laure Bar, Hugues Bonnet, Frédérique Loiseau, Hélène Jamet, Jérôme Dejeu, et al.

Photo-oxidizing ruthenium(II) complexes with enhanced visible light absorption and G-quadruplex binding abilities

Martin Gillard,[a] Guillaume Piraux,[a] Martin Daenen,[a] Michaël Abraham,[a] Ludovic Troian-Gautier,[a] Laure Bar,[b] Hugues Bonnet,[b] Frédérique Loiseau,[b] Hélène Jamet,[b] Jérôme Dejeu,[b] Eric Defrancq,[b] and Benjamin Elias*[a]

Abstract:
Photosensitizers that gather high photo-oxidizing power and strong visible light absorption are of great interest in the development of new photo-chemotherapeutics. Indeed, such compounds constitute attractive candidates for the design of type I photosensitizers that are not dependent on the presence of oxygen. In this paper, we report on the synthesis and studies of new ruthenium(II) complexes that display strong visible light absorption and can oxidize guanine residues under visible light irradiation, as evidenced by nanosecond transient absorption spectroscopy. The reported compounds also tightly bind to G-quadruplex DNA structures from the human telomeric sequence (TTAGGG repeat). The kinetic and thermodynamic parameters of the interaction of these Ru(II) complexes with G-quadruplex and duplex DNA were studied thanks to luminescence titrations and bio-layer interferometry measurements, which revealed higher affinities towards the non-canonical G-quadruplex architecture. Docking experiments and non-covalent ionic analysis allowed to gain information on the mode and the strength of the interaction of the compounds towards G-quadruplex and duplex DNA. The different studies emphasize the substantial influence of the position and the number of non-chelating nitrogen atoms on the interaction with both types of DNA secondary structures.

Introduction

Ruthenium(II) metal complexes offer many appealing assets in the design of photosensitizers for cancer phototherapy thanks to their high stability, strong visible light absorption and long-lived excited states.[1] Ruthenium(II) compounds containing polypyridyl ligands have been the most explored frameworks since the report of the DNA light switch effect of $[Ru(bpy)_2dppz]^{2+}$ (bpy = 2,2′-bipyridine, dppz = dipyrido[3,2-:2′,3′-]phenazine) in the early 90's.[2] Many analogues were developed aiming to enhance the photo-oxidizing properties and to improve the accumulation of the compounds into cancer cells. The enhancement of the photo-oxidizing power of these complexes has been mainly achieved through the addition of nitrogen atoms in the ligands structure. Notably the use of TAP (TAP = 1,4,5,8-tetraazaphenanthrene) or bpz (bpz = 2,2′-bipyrazine) ancillary ligands leads to strong photo-oxidizing complexes able to trigger oxidative electron transfer with DNA (type I photo-oxidation).[3] Developing highly photo-oxidizing sensitizers constitutes interesting alternatives in cancer phototherapy when the type II pathway (ROS photoproduction) is prevented by hypoxia.[4] In order to favour accumulation of the photosensitizers into cancer cells, the association to DNA secondary structures that are present in higher prevalence in many cancer cell lines such as G-quadruplex DNA (G4 DNA) and DNA mismatches has been extensively studied.[5] Therefore, numerous compounds including ruthenium(II) complexes have been designed to bind selectively G4 DNA or DNA mismatches over double stranded DNA.[6] Telomeric G4 DNA has emerged as a promising target for cancer therapy since the discovery of its implication in the cancer cell immortalization process in addition to the major role it plays in the development of the disease.[7]

Recently, we reported on the design of $[Ru(phen)_2dph]^{2+}$ (**1**) (phen = 1,10-phenanthroline, dph = dipyrazino[2,3-a:2',3'-h]phenazine), which showed high selectivity towards G4 over duplex DNA in addition to strong visible light absorption. This was attributed to the extended conjugation of the dph ligand.[8] Based on these interesting results, three analogues (**Figure 1**) were prepared to (i) enhance the conjugation of the extended dph ligand in the $[Ru(phen)_2bpph]^{2+}$ (**2**) complex (bpph = benzo[a]pyrazino[2,3-*h*]phenazine) and to (ii) increase the photo-oxidizing power of the compounds by replacing the phen ancillary ligands by TAP in $[Ru(TAP)_2dph]^{2+}$ (**3**) and $[Ru(TAP)_2bpph]^{2+}$ (**4**).

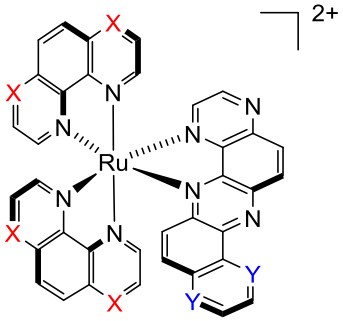

(**1**) X = C, Y = N $[Ru(phen)_2dph]^{2+}$
(**2**) X = C, Y = C $[Ru(phen)_2bpph]^{2+}$
(**3**) X = N, Y = N $[Ru(TAP)_2dph]^{2+}$
(**4**) X = N, Y = C $[Ru(TAP)_2bpph]^{2+}$

Figure 1: Structures of complexes **1-4**.

[a] M. Gillard, G. Piraux, M. Daenen, M. Abraham, Dr. L. Troian-Gautier and Prof. B. Elias
Université catholique de Louvain (UCLouvain)
Institut de la Matière Condensée et des Nanosciences (IMCN), Molecular Chemistry, Materials and Catalysis (MOST)
Place Louis Pasteur 1, bte L4.01.02, 1348 Louvain-la-Neuve (Belgium)
E-mail: Benjamin.Elias@uclouvain.be
[b] Dr. L. Bar, H. Bonnet, Prof. F. Loiseau, Dr. H. Jamet, Dr. J. Dejeu and Prof E. Defrancq
Université Grenoble Alpes (UGA)
Département de Chimie Moléculaire, UMR CNRS 5250
CS 40700 - 38058 Grenoble (France).

The synthesis of compounds **2-4** as well as their photophysical and photochemical properties are reported herein. The interaction of complexes **1-4** with G4 DNA and duplex DNA as well as their excited-state reactivity was investigated by bio-layer interferometry, luminescence titrations, nanosecond transient absorption and computational studies. Strikingly, such weak structural changes between the different analogues led to considerable changes both to the photophysics and the affinity of the compounds towards G4 over duplex DNA.

Results and Discussion

Synthesis

The pyrazine core synthesis of the dph ligand was previously developed by our group. It consists in the coupling of two 6-aminoquinoxaline thanks to an optimized Chichibabin-like reaction (i.e. through an addition–oxidation–elimination mechanism).[8] The dissymmetric bpph ligand was prepared through the dione-diamine condensation of 1,2-naphtoquinone and 5,6-diaminoquinoxaline, as previously reported.[9] Phen- and TAP-based Ru^{II} mononuclear complexes **1-4** (**Figure 1**) were synthesized through the direct chelation of the dph or bpph ligands onto $[Ru(phen)_2Cl_2]$ and $[Ru(TAP)_2Cl_2]$ precursors. The previously reported complex $[Ru(phen)_2(dph)]^{2+}$ **1** as well as new compounds $[Ru(phen)_2(bpph)]^{2+}$ **2**, $[Ru(TAP)_2(dph)]^{2+}$ **3** and $[Ru(TAP)_2(bpph)]^{2+}$ **4** were characterized by NMR spectroscopy and high-resolution mass spectrometry (see the supporting information).

Electrochemical study

The electrochemical characterization of compounds **1-4** allowed to better understand their photophysical and photochemical properties. The data were recorded in acetonitrile containing 0.1 M tetrabutylammonium perchlorate (Bu_4NClO_4) (**Table 1**).

Table 1: Oxidation (E_{ox}) and reduction (E_{red}) potentials of complexes **1–4** in acetonitrile. Estimated reduction potentials (E^*_{red}) of complexes **1–4** in acetonitrile.

Complex	E_{ox}[a][V][b]	E_{red}[a][V][b]	E^*_{red}[a][V][b]
$[Ru(phen)_3]^{2+}$	+1.32	-1.30, -1.47, -1.68	+0.75
$[Ru(phen)_2dph]^{2+}$[1] **1**	+1.63	-0.74, -1.24, -1.67	+0.86
$[Ru(phen)_2bpph]^{2+}$ **2**	+1.60	-0.77, -1.24,-1.66	+0.83
$[Ru(TAP)_3]^{2+}$	+1.98	-0.71, -0.85, -1.15	+1.32
$[Ru(TAP)_2dph]^{2+}$ **3**	>1.8	-0.65, -1.58	+1.21
$[Ru(TAP)_2bpph]^{2+}$ **4**	>1.8	-0.66, -1.55	+1.25

[a] Data were measured at room temperature in MeCN with 0.1 M Bu_4NClO_4 as supporting electrolyte, with a concentration of complexes of 0.8 mM [b] Potentials are given *vs.* Ag/AgCl. Excited-state potentials estimated from the equations: $E^*_{1/2red} = E_{1/2red} + E_{0\text{-}0}$. The energy of the excited state, $E_{0\text{-}0}$, was estimated by Franck–Condon line-shape analysis of the emission spectra at 298 K in MeCN.

Concerning the oxidation, the observed process can be attributed to the oxidation of the metallic centre. It should be noted that complexes **1-2** are less easily oxidized compared to the reference complex $[Ru(phen)_3]^{2+}$. Furthermore, no oxidation process could be monitored for TAP analogues (*i.e.* complexes **3** and **4**) at a potential below 1.8 V, which is consistent with the data reported for the reference complex $[Ru(TAP)_3]^{2+}$.[10] Concerning the ligand-centred reduction processes, compounds **1** and **2** are notably easier to reduce than $[Ru(phen)_3]^{2+}$. The first reduction wave is attributed to the reduction of the dph or bpph ligand. Both TAP analogues **3** and **4** are the easiest to reduce displaying more positive reduction potentials than $[Ru(TAP)_3]^{2+}$. These results indicate that the HOMO of complexes **1-4** is centred on the metal core while their LUMO orbital is localized on the ligands, which is in good agreement with the occurrence of a MLCT transition as suggested by light absorption (*vide infra*) and literature data.

The excited-state reduction potentials were estimated based on the ground-state reduction potentials and the energy stored in the excited state, $E_{0\text{-}0}$. As expected, complexes **3** and **4** display strong photo-oxidizing power (E^*_{red} = +1.21 and +1.25 V *vs.* Ag/AgCl, respectively). This suggests that those compounds should trigger photo-induced electron transfer (PIET) in the presence of a guanine residue (E_{ox}(dGMP) = +1.10 V *vs.* Ag/AgCl), the most oxidizable DNA nucleobase.[11]

Light absorption

The absorption and emission spectra of complexes **1-4** recorded in acetonitrile are shown in **Figure 2**. The corresponding photophysical data along with those of reference compounds $[Ru(phen)_3]^{2+}$ and $[Ru(TAP)_3]^{2+}$ are gathered in **Table 2**.[10]

The absorption spectra show a strong peak at 265 nm for **2** and at 315 nm for its TAP analogue **4**, which is attributed to LC transitions localized on the ligands. Strong absorption bands were also observed in the visible region (in the range 400-500 nm) which are attributed to MLCT transitions. A strong hypsochromic shift of the MLCT transition was observed for complex **2** compared to **1** (**Table 2**) which is consistent with the replacement of two non-chelating nitrogen by carbon atoms in the bpph, accounting for an increase of the LUMO orbital energy level. The large bathochromic shifts (> 40 nm) of the MLCT transitions observed for the complexes **1-4** compared to the reference complexes $[Ru(phen)_3]^{2+}$ and $[Ru(TAP)_3]^{2+}$ are of great interest for the proposed applications and most likely arise from the high conjugation of the dph and bpph ligands.

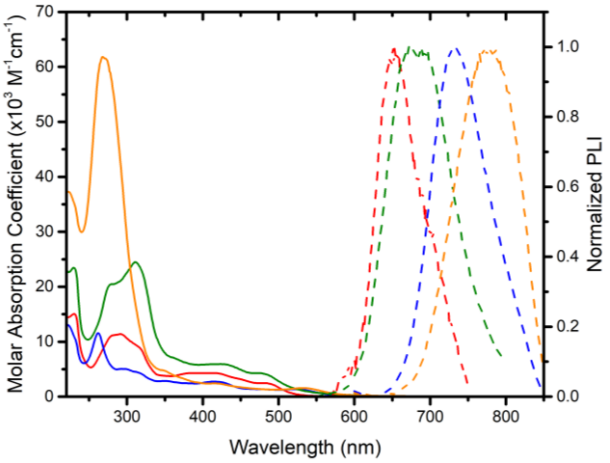

Figure 2. Absorption (solid line) and emission (dashed line) spectra of $[Ru(phen)_2dph]^{2+}$ **1** (orange), $[Ru(phen)_2bpph]^{2+}$ **2** (blue), $Ru(TAP)_2dph]^{2+}$ **3** (green) and $[Ru(TAP)_2bpph]^{2+}$ **4** (red) in acetonitrile at room temperature.

Table 2: Absorption and emission data in acetonitrile for complexes **1-4** at 298 K.

Complex	λ_{Abs} [nm] (ε)[a]	λ_{Em} [nm][b]	τ[ns][c]	Φ[d]	k_r [10^3 s^{-1}][e]
$[Ru(phen)_3]^{2+}$	447	604	460	0.028	60.9
$[Ru(phen)_2dph]^{2+}$[1] **1**	530 (1.5)	773	380	0.0016	4.21
$[Ru(phen)_2bpph]^{2+}$ **2**	524 (1.7)	727	100	0.0084	84
$[Ru(TAP)_3]^{2+}$	435 (16)	580	420	0.012	28.6
$[Ru(TAP)_2dph]^{2+}$ **3**	479 (4.2)	667	701	0.0172	24.5
$[Ru(TAP)_2bpph]^{2+}$ **4**	482 (2.5)	650	460	0.0084	18.3

[a] λ_{Abs} corresponds to the most bathochromic transition in MeCN (extinction coefficient, ε x10^3 $M^{-1}cm^{-1}$). [b] Emission wavelength (λ_{Em}) recorded in MeCN at RT. [c] Luminescence lifetime in MeCN under argon at RT. [d] quantum yield of emission measured by comparison with the reference $[Ru(bpy)_3]^{2+}$. [e] k_r: the radiative deactivation rate constant.

Light emission

The four complexes **1-4** display strong visible light emission with quantum yields, excited state lifetimes and large k_r values (> 10^3 s^{-1}) (**Table 2**) that suggest a ^{3}MLCT-type emitting state as already reported for similar Ru^{II} compounds.[8] Complexes **1-4** exhibit large bathochromic shifts of their emissions (>40 nm) compared to the reference compounds, which could be due to the high conjugation of the dph and bpph ligands. Interestingly, bpph containing complexes **2** and **4** show emission at higher energies than the corresponding dph containing compounds **1** and **3**, which can be explained by the low-lying LUMO of the dph containing complexes. In addition, the fact that dph containing compounds **1** and **3** possess longer luminescence lifetimes than the corresponding bpph containing analogues **2** and **4** can be related to a smaller contribution of the non-radiative decay on the overall emission process in the dph complexes**.** Complexes **3** and **4** bearing TAP ancillary ligands exhibit strongly blue shifted emission compared to their phen analogues. The recorded emission wavelengths for compounds **3** and **4** are similar to those reported for other complexes containing TAP ancillary ligands. The luminescence lifetimes of the TAP containing compounds **3** and **4** are also noticeably longer than those of their respective phen analogues **1** and **2**, as anticipated.

dGMP photo-oxidation

As suggested by the electrochemical and photophysical studies, the presence of two TAP ancillary ligands in compounds **3** and **4** leads to complexes with enhanced photo-oxidation capacities compared to **1** and **2**. This was highlighted by the assessment of their reduction potentials in the excited state (**Table 1**). Therefore, the ability of complexes **3** and **4** to oxidize deoxyguanosine monophosphate (dGMP) under light irradiation was explored by luminescence quenching experiments. As depicted in Figure **3**, a dramatic luminescence decrease was observed through the gradual addition of dGMP to a buffered solution of compounds **3** and **4.**

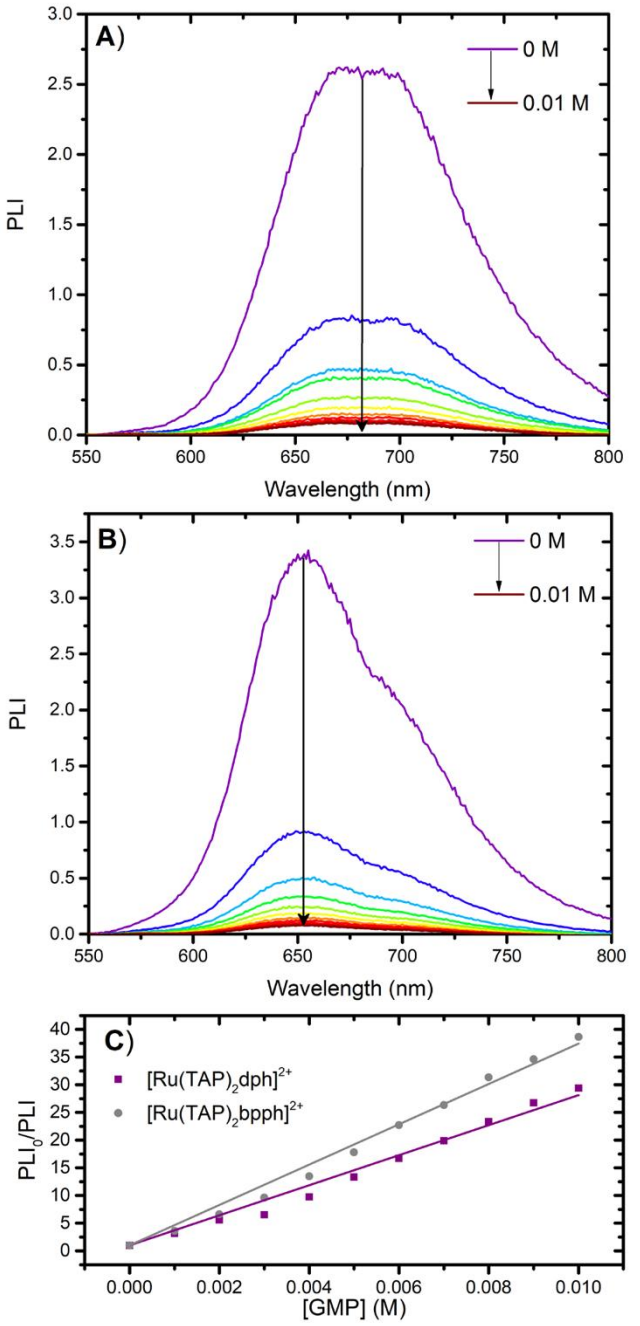

Figure 3: Evolution of the luminescence spectra of (**A**) $[Ru(TAP)_2dph]^{2+}$ **3** (λ_{exc} = 479 nm), (**B**) $[Ru(TAP)_2bpph]^{2+}$ **4** (λ_{exc} = 482 nm) in the presence of increasing concentrations of dGMP, while the complex concentration was kept at 5 µM.. Measurements were made in 50 mM Tris·HCl, 50 mM NaCl, pH = 7.4, under ambient air conditions. Insets: Stern–Volmer plots obtained upon the addition of dGMP to each complex.

Gibbs free energy variations (ΔG) corresponding to the electron transfer process (ET) from a guanine moiety to the excited complexes **3** and **4** were estimated from voltametric and photophysical data. The spontaneity of the ET process was thereby confirmed with calculated ΔG_{ET} ranging between -0.15 and -0.19 eV. The ΔG_{ET} were also calculated against a guanine rich Poly(dG-dC)$_2$ sequence to assess the impact of the guanine stacking, which is known for making the photo-oxidation process even more favoured (**Table 3**). The efficiency of the luminescence quenching (k_q) was determined thanks to Stern-Volmer relationship (**Figure 3** - insets). The linearity of the

Stern-Volmer plot indicates a pure dynamic quenching of the excited state of the two complexes by dGMP and the obtained k_q values (**Table 3**) shows a diffusion rate limited process.[12] This efficient luminescence quenching is in agreement with a PIET process occurring between excited TAP containing complexes **3** and **4** and the guanine base. It also points out the ability of dph and bpph TAP-based complexes for DNA photo-oxidation.

Table 3: Photo-induced ET from guanine-based moieties to **3** and **4**.

	ΔG_{ET} [eV][a]		
Compound	dGMP	Poly(dG-dC)$_2$[c]	k_q [M^{-1} s^{-1}][b]
$[Ru(TAP)_2dph]^{2+}$ **3**	-0.15	-0.40	2.20 x 10^9
$[Ru(TAP)_2bpph]^{2+}$ **4**	-0.19	-0.44	3.02 x 10^9

[a] Gibbs free energy variation corresponding to the ET process from guanine to the excited complex estimated as $\Delta GET = -nF(E_{Ru2+*/Ru+} - E_{G\bullet+/G})$, with $E_{G\bullet+/G}$ = +1.10 V for dGMP or +0.85 V for Poly(dG-dC)$_2$ and $E_{Ru2+*/Ru+}$ = E*red values in Table 1. [b] Quenching rate constant (kq) obtained using the Stern–Volmer equation $I_0/I = 1 + k_{qT0}[dGMP]$. I_0/I (where I_0 is the luminescence of the complex in the absence of a quencher, here dGMP, and I is the luminescence in the presence of dGMP) as a function of the quencher concentration; τ0, the excited state lifetime of the complex in the absence of dGMP. [c] ΔG_{ET} values with Poly(dG-dC)$_2$ are given for comparison purpose in order to indicate the effect of the guanine stack.

Time-resolved spectroscopies were then used to obtain further information about the light-induced quenching processes. The experiments were carried out in argon-purged buffered solutions using $[Ru(TAP)_2bpph]^{2+}$. The excited-state quenching with dGMP was first repeated as the excited-state lifetime of $[Ru(TAP)_2bpph]^{2+}$ in 50 mM Tris·HCl, 50 mM NaCl and pH = 7.4 was determined as 3.1 µs. Upon the addition of dGMP, a drastic decrease of the excited-state lifetime was observed (**Figure 4A**). The corresponding Stern-Volmer plot was linear and allowed to determine the quenching rate constant, k_q = 2.45 x10^9 $M^{-1}s^{-1}$. This agrees with the quenching rate constant determined via steady-state spectroscopy.

We then turned to nanosecond transient absorption spectroscopy. The excited state absorption features of $[Ru(TAP)_2bpph]^{2+}$ were in line with prototypical Ru(II) complexes, i.e. a strong bleaching observed in the visible part of the spectrum, corresponding to light oxidation of Ru(II) to Ru(III) and positive absorption features in the UV and red region of the spectrum, in agreement with the formation of a reduced ligand (**Figure 4B**). This is fully consistent with the metal-to-ligand charge transfer (MLCT) nature of the excited state. The excited-state reactivity with dGMP was then investigated using pulsed 480 nm light excitation. The transient absorption spectra recorded 200 ns after the laser pulse were fully consistent with excited-state electron transfer, generating the monoreduced complex and oxidized dGMP. Similar experiments were then conducted using G4. The spectral signatures observed 500 ns after the laser pulse matched those obtained using dGMP, indicative of the efficient photo-induced excited-state electron transfer between $[Ru(TAP)_2bpph]^{2+*}$ and G4. Note that the signal for that experiment presents larger signal/noise ration below 400 nm. This is a consequence of the experimental setup as a volume of 300 µL was used in a 0.3x0.3cm cuvette. Nevertheless, the transient absorption features unambiguously confirm the photo-induced oxidative electron transfer from dGMP or guanine residue in G4 to the excited complex.

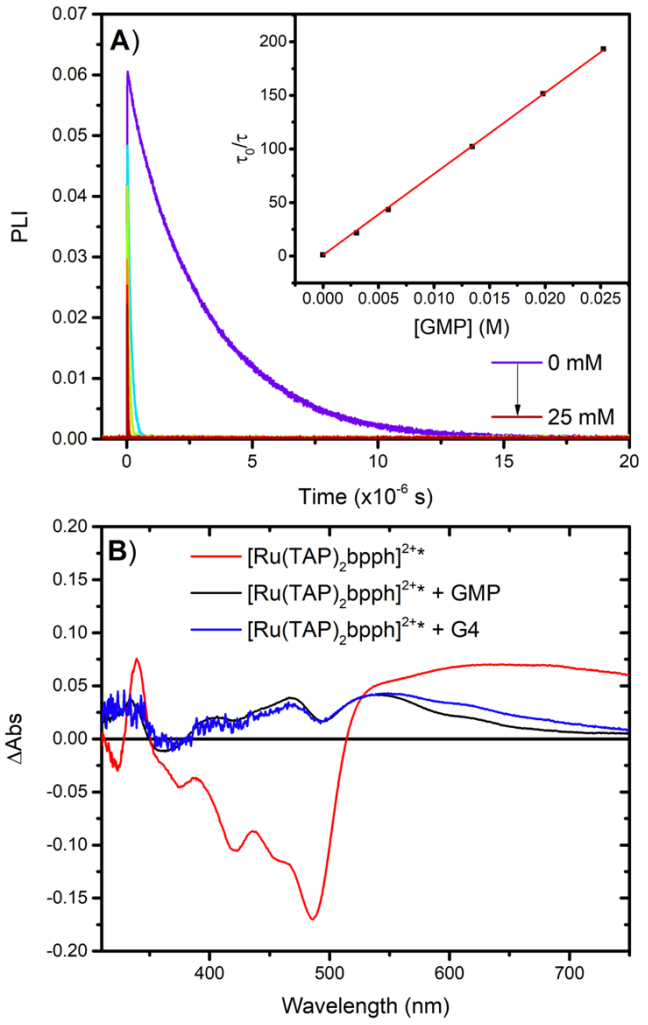

Figure 4: (**A**) Time-resolved excited-state quenching of $[Ru(TAP)_2bpph]^{2+}$ with increasing amount of dGMP. The inset shows the corresponding Stern-Volmer plot from which k_q = 2.45 x10^9 $M^{-1}s^{-1}$ was determined. (**B**) Transient absorption spectroscopy of $[Ru(TAP)_2bpph]^{2+}$ (red), $[Ru(TAP)_2bpph]^{2+}$ with 10 mM of dGMP (black) and $[Ru(TAP)_2bpph]^{2+}$ with 43 µM G4 (red) recorded 200 ns (integrated for 100 ns) following pulsed 480 nm light excitation. The experiments using G4 were recorded in 10 mM HEPES, pH 7.5, 50 mM NaCl, 100 mM KCl under argon whereas the other experiments were recorded in 50 mM Tris·HCl, 50 mM NaCl, pH = 7.4, under argon.

DNA interaction studies

Luminescence titrations, bio-layer interferometry analysis (BLI) and computational studies were implemented to study the interaction of complexes **1-4** towards duplex and G4 DNA. Overall, these experimental methods allowed to measure the affinity and selectivity of the compounds for G4 DNA secondary structure, in addition to characterize the interactions occurring with both duplex and G4 DNA. For DNA titrations, calf thymus DNA (CT-DNA) and wtTel23 were chosen as duplex and G4 DNA models respectively. For BLI, biotinylated versions of GC-rich duplex and wtTel23 sequence were chosen (see **Figure 5 A and 5 B**). It must be noted that while calf thymus DNA contains an equivalent molar amount of the four DNA bases, the GC-rich hairpin model is richer in guanine and cytosine.

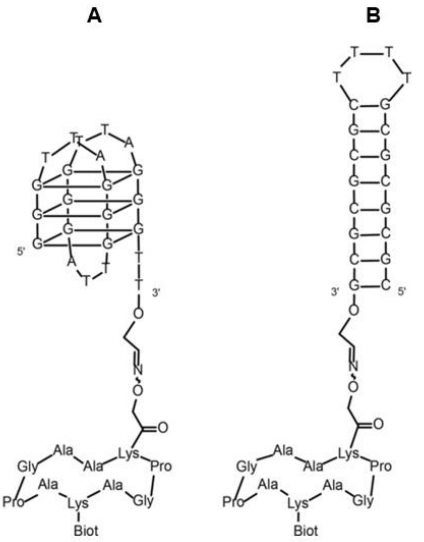

Figure 5: Biomolecular models used for bio-layer interferometry studies: **A**, intramolecular G-quadruplex structure; **B**, duplex DNA hairpin.

Luminescence titrations

While enhanced luminescence was observed for phen containing complexes **1** and **2** in the presence of increasing concentration of CT and G4 DNA (**Figure 6A**), a decrease of the luminescence was observed for TAP containing complexes **3** and **4** (**Figure 6B**). The luminescence increase observed for both complexes **1** and **2** upon addition of DNA can be related to a light switch type effect as reported for $[Ru(bpy)_2dppz]^{2+}$.[1] This behaviour is explained by an efficient protection of the ^{3}MLCT excited state from non-radiative decay sources such as solvent molecules and dioxygen when interacting with DNA. The strong decrease of luminescence intensity for both complexes **3** and **4** show that complexes **3** and **4** are potential photoreactive equivalents of complexes **1** and **2**, respectively.

Binding affinity constants were estimated using a modified McGhee–von Hippel equation (lines and dashed lines in **Figure 6A and 6B**), expressing the luminescence intensity as a function of the ratio of Ru^{II} compound per DNA site (I/I_0 vs. [Site]/[Ru]), with I_0, the intensity of luminescence in the absence of DNA and [Site] referring either a base-pair or a G4 equivalent (**Table 4**). Interestingly, higher affinities towards CT-DNA were observed when the two non-chelating nitrogen of dph (complexes **1** and **3**) were removed (complexes **2** and **4**).

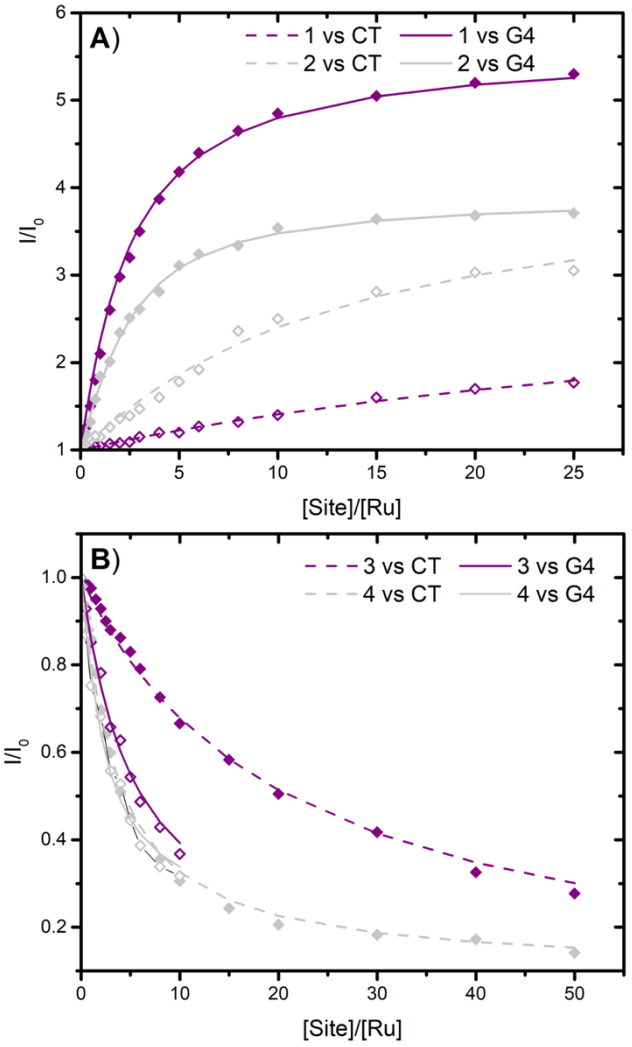

Figure 6: Steady state photoluminescence titration of (**A**) $[Ru(phen)_2dph]^{2+}$ **1** (purple) and $[Ru(phen)_2bpph]^{2+}$ **2** (grey) and (**B**) $[Ru(TAP)_2dph]^{2+}$ **3** (purple) and $[Ru(TAP)_2bpph]^{2+}$ **4** (grey) by increasing G4-DNA (full diamonds) or ds-DNA (empty diamonds) ratio, while the complex concentration was kept at 5 µM. The fitted curves are obtained using a modified McGhee–von Hippel equation (see the SI) and drawn as solid and dashed curves for G4 and ds-DNA respectively. One site in ds-DNA corresponds to one base pair and to one quartet in G4 structures and I_0, the photoluminescence of the complex in the absence of DNA. λ_{exc} = 450 nm; λ_{Em} = 773 (**1**), 727 (**2**), 667 (**3**) and 650 nm (**4**).

Table 4: Equilibrium dissociation constants (K_D) for the interaction of complexes **1**-**4** with G4 and duplex DNA estimated from steady state luminescence titrations.

	G4 DNA (wtTel23)		Duplex DNA (CT-DNA)	
Compound	K_D (µM)	I/I_0 max	K_D (µM)	I/I_0 max
$[Ru(phen)_2dph]^{2+}$ **1**	18.9	4.9	652	1.8
$[Ru(phen)_2bpph]^{2+}$ **2**	14.6	3.7	91	3.1
$[Ru(TAP)_2dph]^{2+}$ **3**	31.7	0.36	198	0.28
$[Ru(TAP)_2bpph]^{2+}$ **4**	19.1	0.32	31	0.14

Binding constants are obtained using a McGhee–von Hippel type equation; the binding site corresponds to base pair or G-quartet (best fit). Errors estimated to 5%.

Bio-layer interferometry

Bio-layer interferometry (BLI) was implemented to gain access to the more accurate dissociation equilibrium constant of the interactions (K_D) *via* the measurements of kinetics of association (k_{on}) and dissociation (k_{off}). Two DNA structures were used as models: the intramolecular G-quadruplex **Figure 5A** (HTelo sequence, in equilibrium between the different topologies), and the duplex DNA model **Figure 5B** (hairpin structure). These structures have been already used for the study of interactions of putative ligands with G4 and duplex DNA.[6b, 8] The binding constants for complexes **1-4** are reported in **Table 5**. The measured K_D value for the interaction of complex **1** with G4 DNA is in the micromolar range (9 µM) while no equilibrium constant could be calculated for the interaction with the duplex DNA. This is in agreement with the previously reported results obtained from surface plasmon resonance analyses and confirms the selectivity of complex **1** towards G4 over double-stranded DNA structures.[8] Replacing the phen ancillary ligands of complex **1** by TAP in complex **3** led to a dramatic decrease of the affinity towards G4 DNA (K_D = 66 µM) which could be attributed to both a slower association (factor 2) and a faster dissociation (factor 4) according to the kinetic constants (**Figure 7** and **Table 5**). However, the selectivity towards G4 *vs.* duplex DNA structures remains as no equilibrium constants could be measured for the interaction with the duplex DNA hairpin. These results were concordant with the luminescence titrations.

The removal of two non-chelating nitrogen atoms from the dph ligand in complex **1** to form the bpph ligand in complex **2** also led to a huge impact on the interactions with G4 and duplex DNA. Indeed, a decrease of the affinity towards G4 was observed (K_D = 32 µM) while a weak affinity for duplex DNA could be measured (K_D = 102 µM) thus leading to a partial loss of the selectivity towards G4 DNA. Nevertheless, it is noteworthy that the measured K_D value for duplex DNA being far beyond the studied concentration range (due to solubility problems), its accuracy must be taken with care. For complex **4** which contains both bpph and tap ligands, the selectivity towards G4 strongly decreased due to a higher affinity of the compound for duplex DNA.

The comparison of the kinetic parameters measured for the interactions of bpph containing complexes **2** and **4** showed a slower dissociation rate when interacting with G4 compared to duplex DNA (0.5 s^{-1} *versus* 1.4-1.8 s^{-1}). However, for complex **4** a higher association rate was observed for duplex *versus* G4 DNA (8.1 10^4 $M^{-1}s^{-1}$ and 2.7 10^4 $M^{-1}s^{-1}$, respectively) thus leading to the partial loss of selectivity. The affinity distribution can be better visualized in **Figure 6**.

It emerges from these results that the number of non-chelating nitrogen atoms and their position have a considerable impact on the interactions with both G4 and duplex DNA. This parameter appears to play a determining role on the interaction strength and on the selectivity of the compounds for G4 *versus* duplex DNA structures. In this context, we decided to perform a computational study of the interaction with the aim to explain the observed differences.

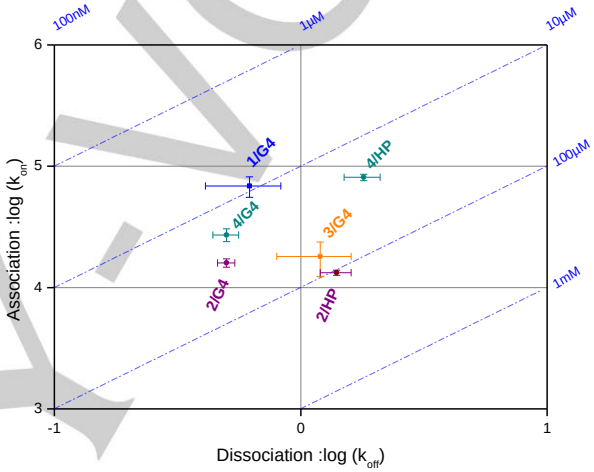

Figure 7: Isoaffinity kinetic plot of rate constants measured by BLI. The dashed diagonals depict the equilibrium binding constants and are shown to help with the visualization of the affinity distribution. Complexes **1** and **3** are plotted in the presence of G4 DNA (G4) and complexes **2** and **4** both in presence of G4 DNA and duplex DNA hairpin (HP).

Table 5: Equilibrium dissociation constants (K_D) for the interaction of complexes **1-4** with G4 and duplex DNA measured from bio-layer interferometry analysis.

Complex	G4 DNA			Duplex DNA		
	k_{on} [10^4 $M^{-1}.s^{-1}$]	k_{off} [s^{-1}]	K_D [µM][a]	k_{on} [10^5 $M^{-1}.s^{-1}$]	k_{off} [s^{-1}]	K_D [µM][a]
$[Ru(phen)_2dph]^{2+}$ **1**	6.6 ± 1.3	0.6 ± 0.2	9 ± 2	n.d.[b]	n.d.[b]	n.d.[b]
$[Ru(phen)_2bpph]^{2+}$ **2**	1.6 ± 0.1	0.5 ± 0.04	32 ± 4	1.3 ± 0.06	1.4 ± 0.2	102 ± 22
$[Ru(TAP)_2dph]^{2+}$ **3**	1.8 ± 0.6	1.2 ± 0.4	66 ± 15	n.d.[b]	n.d.[b]	n.d.[b]
$[Ru(TAP)_2bpph]^{2+}$ **4**	2.7 ± 0.3	0.5 ± 0.06	19 ± 2	8.1 ± 5.0	1.8 ± 0.3	37 ± 22

[a] Equilibrium dissociation constants were deduced from the kinetic rate constants. [b] Due to the very low binding of the complex with duplex DNA, the kinetics of the interaction could not be determined (n.d.) in the studied concentration range. Measurements were performed using a concentration range from 5 µM to 40 µM of the complexes in 10 mM HEPES pH 7.5, 50 mM NaCl, 100 mM KCl and 0.05% v/v P20 surfactant.

Computational studies

The interactions arising between complexes **1-4** and their DNA targets, namely duplex and G-quadruplex, were investigated through docking experiments. The choice of the structures used for the targets is explained in the experimental computational part.

Docking studies were performed using the AutoDock 4.0 software package.[13] Different positions were generated and ranked in a histogram according to a scoring function correlated to the interactions. The analysis of the best-ranked docked positions gives similar results for all the four complexes. Regarding the hairpin, two binding modes emerge: a more stable one where the complex interacts within the minor groove, and a slightly less stable one in which the extended planar ligand dph or bpph is inserted inside the loop. **Figure 8a** shows these two binding modes for complex **1** with their scoring function.

In the G4 structure, two positions were also obtained: a more stable interaction involving the insertion of the extended planar dph or bpph ligand inside one of the grooves, and a less stable one where the extended planar dph or bpph ligand is stacked over the guanine tetrad (**Figure 8b for complex 1**).

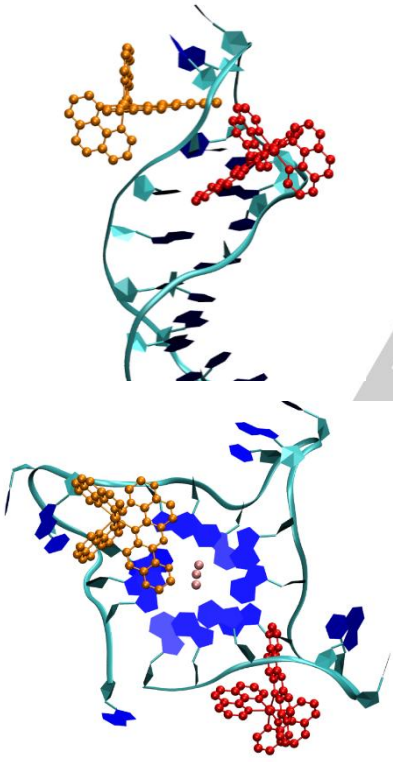

Figure 8: The main docked positions of complex **1** **(a)** against a hairpin structure, inside the T-loop (orange, scoring function -4.45 kcal/mol) or in the minor groove (red, scoring function -4.25 kcal/mol), **(b)** against a human G-quadruplex (PDB entry 1KF1), stacked above a G quartet (orange, scoring function -4.45 kcal/mol) or embedded in the groove (red, scoring function -6.22 kcal/mol).

Interestingly, the mean binding energies of the more stable interactions obtained by docking are consistently lower for the G-quadruplex than for the hairpin, suggesting that favored for the G4 over the hairpin structure. This observation is consistent with the luminescence titrations and BLI analysis results that gave lower K_D values for the G4 for each complex assessed. Furthermore, theoretical dissociation constants were calculated upon introduction of the mean binding energies in

$$K_D{}^{-1} = exp\left(\frac{-\Delta G^{\circ}}{RT}\right)$$

with T = 298.15K, giving K_D values in the order of magnitude of 100 µ M, in agreement with the BLI experiments.

Finally, the interactions were visualized through a non-covalent interaction (NCI) analysis in the quadruplex, highlighting the regions associated with specific interactions of various strengths; from steric repulsion (red), van der Waals interactions (green), to strong attractions (blue).

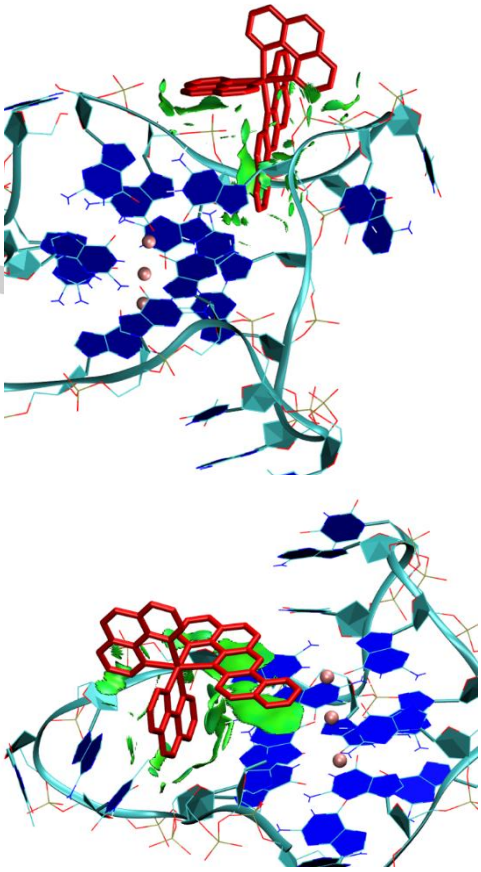

Figure 9: NCI surfaces obtained for the complex **1** (red) in interaction with the human G-quadruplex (PDB entry 1KF1), the gradient cut-off is 0.45 u.a. and the colour scale set to <0.07 u.a.; **(a)** interaction within the G-quadruplex groove, **(b)** π-stacked position over the G-tetrad.

Thus, the NCI analysis for the docked position inside the G4s groove showed that the main interactions arise from vdW interactions mostly located around the embedded extended planar ligand. As for the stacked position, the NCI analysis confirms a large π-π stacking interaction as well as some vdW interactions with one of the ancillary ligands facing towards the G-tetrads (**Figure 9**). However, no significant difference was observed amongst the four complexes and no additional interactions were found between the two additional non-chelating nitrogen's in the dph containing compounds **1** and **3** compared to their bpph analogs **2** and **4**, so the NCI analysis cannot account for the variations of the K_D observed experimentally.

Conclusion

In this paper, the synthesis of three new Ru(II) complexes **2-4** is reported. That includes the interesting dissymmetric bpph ligand and two photo-oxidizing TAP analogues. The designed compounds photophysical properties were studied by electrochemistry, UV/Vis absorption and emission spectroscopy. The results show the compatibility between the dph and bpph ligands and the presence of TAP ancillary ligands to provide strongly photo-oxidizing compounds. It also appeared that Ru(II) complexes **3** and **4** gather high photo-oxidizing power ($E^*_{1/2red}$ > 1.2 V) and strong visible light absorption (ε = 2800 and 5200 M^{-1} cm^{-1} at 480 nm) thanks to a rational ligand design. Compounds **3** and **4** can photo-oxidize dGMP under visible light irradiation (λ_{exc} = 480 nm) via PIET, as evidenced by nanosecond transient absorption spectroscopy. This PIET occurred with high quenching constant values ($k_q > 10^9$ M^{-1} s^{-1}). Luminescence titrations and BLI analysis allowed to gain access to the kinetic and thermodynamic parameters of the interaction. The two implemented techniques gave concordant results that highlight the substantial influence of the non-chelating nitrogen numbers and position on the interaction with both G4 and duplex DNA. The dph analogues **1** and **3** appeared to be slightly more selective towards G4 *vs*. duplex DNA compared to their respective bpph analogues **2** and **4.** Computational studies describing the interactions between the four complexes and the two targets revealed two binding modes and confirmed higher interactions with the G4 compared to the hairpin structures.

Experimental Section

Materials and instrumentation

$[Ru(phen)_2Cl_2]$, $[Ru(TAP)_2Cl_2]$, $[Ru(phen)_2dph]^{+2}$ **1** and bpph were synthesized according to previously described literature protocols.[8-9] All solvents and reagents for the synthesis were of reagent grade and were used without any further purification. All solvents for the spectroscopic and electrochemical measurements were of spectroscopic grade. Water was purified with a Millipore Milli-Q system. Calf thymus DNA Type I (CT-DNA) was purchased from Sigma-Aldrich. ^1H and ^{13}C NMR experiments were performed in $CDCl_3$, CD_3OD or CD_3CN on a Bruker AC-300 Advance II (300 MHz) or on a Bruker AM-500 (500 MHz) at 20°C. The chemical shifts (given in ppm) are measured *vs* the residual peak of the solvent as the internal standard. High-resolution mass spectrometry (HRMS) spectra were recorded on a Q-Extractive orbitrap from ThermoFisher using reserpine as internal standard. Samples were ionized by electrospray ionization (ESI; capillary temperature = 320°C, vaporizer temperature = 320°C, sheath gas flow rate = 5 mL/min).

UV−vis absorption spectra were recorded on a Shimadzu UV-1700. Room temperature luminescence spectra were recorded on a Varian Cary Eclipse instrument. Luminescence intensity at 77 K was recorded on a FluoroLog3 FL3-22 from Jobin Yvon equipped with an 18V 450 W Xenon Short Arc lamp and an R928P photomultiplier, using an Oxford Instrument Optistat DN nitrogen cryostat controlled by an Oxford Intelligent Temperature Controller (ITC503S) instrument. Luminescence lifetime measurements were performed after irradiation at λ = 400 nm obtained by the second harmonic of a Titanium:Sapphire laser (picosecond Tsunami laser spectra physics 3950-M1BB+39868-03 pulse picker doubler) at an 80 kHz repetition rate. The Fluotime 200 from AMS technologies was used for the decay acquisition. It consists of a GaAs microchannel plate photomultiplier tube (Hamamatsu model R3809U-50) followed by a time- correlated single photon counting system from Picoquant (PicoHarp300). The ultimate time resolution of the system is close to 30 ps. Luminescence decays were analysed with FLUOFIT software available from Picoquant. Cyclic voltammetry was carried out in a one-compartment cell, using a glassy carbon disk working electrode (approximate area = 0.03 cm^2), a platinum wire counter electrode, and an Ag/AgCl reference electrode. The potential of the working electrode is controlled by an Auto lab PGSTAT 100 potentiostat through a PC interface. The cyclic voltammograms were recorded with a sweep rate of 300 mV s^{-1}, in dried acetonitrile (Sigma- Aldrich, HPLC grade). The concentration of the complexes was 8.10^{-4} mol/L, with 0.1 mol/L tetrabutylammonium perchlorate as supporting electrolyte. Before each measurement, the samples were purged by nitrogen. Redox potentials were controlled by comparison with ferrocene, added at the end of the measurement.

Synthesis

$[Ru(phen)_2bpph]^{2+}$ **2**. $[Ru(TAP)_2Cl_2]$ (17 mg, 0.0317 mmol) and (Benzo[a]pyrazino[2,3-h]phenazine) (9 mg, 0.0318 mmol) were dissolved ethylene glycol (2 mL) and heated at 120 °C for 5h. After cooling to room temperature, a solution of $NH_4PF_{6\ (aq)}$ (2 mL) was added and the mixture was left over night at 5 °C. The resulting mixture was centrifuged and the solid was washed successively with H_2O, EtOH and diethylether, which gave the final product as a red powder. **^1H NMR (300 MHz, CD_3CN) δ** 9.51 (d, J = 7.8 Hz, 1H), 8.84 (d, J = 2.9 Hz, 1H), 8.81 (d, J = 9.4 Hz, 1H), 8.73 – 8.65 (m, 3H), 8.62 (d, J = 9.4 Hz, 1H), 8.54 (dd, J = 8.3, 1.3 Hz, 1H), 8.31 (d, J = 1.6 Hz, 2H), 8.28 (dd, J = 5.3, 1.3 Hz, 1H), 8.27 – 8.17 (m, 2H), 8.14 (dd, J = 5.3, 1.3 Hz, 1H), 8.00 – 7.86 (m, 4H), 7.78 – 7.65 (m, 4H), 7.64 – 7.49 (m, 3H), 7.02 (d, J = 9.7 Hz, 1H). HR-MS Calcd for $C_{42}H_{26}N_8PF_6Ru$: 889.09679 Da, found 889.09687 Da.

$[Ru(TAP)_2dph]^{2+}$ **3**. $[Ru(TAP)_2Cl_2]$ (20 mg, 0.0373 mmol) and dipyrazino[2,3-a:2',3'-h]phenazine (12.8 mg, 0.0451 mmol) were dissolved in EtOH/H_2O (5 mL/ 1:1) and heated at reflux for 24h. After cooling to room temperature and addition of CH_3CN (2 mL) and H_2O (2 mL), the mixture was centrifuged. NH_4PF_6 was added and the organic solvents were evaporated under vacuum. The resulting mixture was centrifuged and the solid was washed successively with H_2O, EtOH and diethylether to give the crude product. Purification over preparative chromatography on silica ($CH_3CN/H_2O/NH_4Cl_{sat}$ 4/4/1, v/v/v) gave the final product as a red powder. **^1H NMR (500 MHz, CD_3CN) δ** 9.25 (d, *J* = 2.0 Hz, 1H), 9.15 (d, *J* = 2.0 Hz, 1H), 9.10 (d, *J* = 2.8 Hz, 1H), 9.00 (d, *J* = 2.9 Hz, 1H), 8.87 (d, *J* = 2.8 Hz, 1H), 8.75 (d, *J* = 9.5 Hz, 1H), 8.71 (d, *J* = 9.4 Hz, 1H), 8.69 (d, *J* = 9.4 Hz, 1H), 8.62 (d, *J* = 9.4 Hz, 1H), 8.56 (d, *J* = 9.4 Hz, 1H), 8.50 (d, *J* = 2.8 Hz, 1H), 8.45 (d, *J* = 2.8 Hz, 1H), 8.06 (d, *J* = 2.9 Hz, 1H), 8.00 (d, *J* = 9.9 Hz, 2H), 8.00 (d, *J* = 2.7 Hz, 1H), 7.87 (d, *J* = 2.8 Hz, 1H), 7.35 (d, *J* = 9.9 Hz, 1H). HR-MS Calcd for $C_{36}H_{20}N_{14}PF_6Ru$: 895.06807 Da, found 895.06822 Da.

$[Ru(TAP)_2bpph]^{2+}$ **4**. $[Ru(TAP)_2Cl_2]$ (17 mg, 0.0317 mmol) and (Benzo[a]pyrazino[2,3-h]phenazine) (9 mg, 0.0318 mmol) were

dissolved ethylene glycol (2 mL) and heated at 120 °C for 16h. After cooling to room temperature and the addition of a solution of $NH_4PF_{6\,(aq)}$ (2 mL), the mixture was left over night at 5°C. The resulting mixture was centrifuged and the solid was washed successively with H2O, EtOH and diethylether to the final product as a red powder. **^{1}H NMR (300 MHz, CD_3CN) δ 9**.51 (d, *J* = 7.7 Hz, 1H), 9.08 (d, *J* = 2.8 Hz, 1H), 8.95 (t, *J* = 2.5 Hz, 3H), 8.89 – 8.84 (m, 2H), 8.75 – 8.65 (m, 3H), 8.62 – 8.52 (m, 2H), 8.49 (dd, *J* = 2.8, 1.1 Hz, 2H), 8.04 – 7.92 (m, 5H), 7.88 – 7.82 (m, 2H), 6.99 (d, *J* = 9.6 Hz, 1H).

Electrochemical studies

Cyclic voltammetry was carried out in a one-compartment cell, using a glassy carbon disk working electrode (approximate area 0.03 cm^2), a platinum wire counter electrode, and an Ag/AgCl reference electrode. The potential of the working electrode was controlled by an Autolab PGSTAT 100 potentiostat through a PC interface. Cyclic voltammograms were recorded at a sweep rate of 100 mVs^{-1} from solutions in dry acetonitrile (Sigma–Aldrich, HPLC grade). The concentration of the complexes was $8x10^{-4}$ mol L^{-1}, with 0.1 mol L^{-1} tetrabutylammonium perchlorate as supporting electrolyte. Before each measurement, the samples were purged with nitrogen. Redox potentials were determined by comparison with ferrocene, added at the end of the measurement. Luminescence titration experiments with ODNs (GC-rich hairpin or wtTel23 G-quadruplex DNA) were conducted by recording spectra from solutions in 10 mM HEPES, 50 mM NaCl, 100 mM KCl (pH 7.4) buffer on a Varian Cary Eclipse instrument. Titrations were performed by starting from the highest DNA concentration and progressively decreasing it, whilst the concentration of the complex (5 µm) was kept constant.

Photophysical measurements and luminescence titrations

UV/Vis absorption spectra were recorded on a Shimadzu UV-1700 spectrophotometer. Room temperature luminescence spectra were recorded on a Varian Cary Eclipse instrument. Luminescence intensity at 77 K was recorded on a FluoroLog 3 FL3-22 from Jobin Yvon equipped with an 18 V 450 W short-arc xenon lamp and an R928P photomultiplier, using an Oxford Instruments Optistat DN nitrogen cryostat controlled by an Oxford Intelligent Temperature Controller (ITC503S). Quantum yields were obtained using $[Ru(bpy)_3]^{2+}$ as a reference.[14] Luminescence lifetime measurements were performed after irradiation at λ=450 nm obtained as the second harmonic of a titanium: sapphire laser (picosecond Tsunami laser Spectra at a repetition rate of 80 kHz. A Fluotime 200 instrument from AMS Technologies was used for the decay acquisition. It consists of a GaAs microchannel plate photomultiplier tube (Hamamatsu model R3809U-50) followed by a time-correlated single-photon counting system from Picoquant (PicoHarp300). The ultimate time resolution of the system is close to 4 ps. Luminescence titration experiments with ODNs (GC-rich hairpin or wtTel23 G-quadruplex DNA) were conducted by recording spectra from solutions in 10 mM HEPES, 50 mM NaCl, 100 mM KCl (pH 7.4) buffer on a Varian Cary Eclipse instrument. Titrations were performed by starting from the highest DNA concentration and progressively decreasing it, whilst the concentration of the complex (5 µm) was kept constant.

Nanosecond transient absorption

Nanosecond transient absorption measurements were recorded on a previously described apparatus.[15] Briefly, a LP920-K spectrometer from Edinburgh Instruments equipped with an iCCD detector from Andor was used. The excitation source was a tunable Nd:YAG Laser NT342 Series from EKSPLA. The third harmonic (355 nm) at 150 mJ was directed into an optical parametric oscillator (OPO) to enable wavelength tuning starting from 410 nm. The laser power at 480 nm was then attenuated to reach appreciable signal/noise (typically 10 mJ/pulse) and the integrity of the samples was verified by UV-Vis measurements. All samples were recorded in argon-purged buffered aqueous (either 10 mM HEPES, pH 7.5, 50 mM NaCl, 100 mM KCl or 50 mM Tris·HCl, 50 mM NaCl, pH = 7.4) at room temperature.

Bio layer interferometry (BLI)

BLI sensors coated with streptavidin (SA sensors) were purchased from Forte Bio (PALL). Prior to use, they were immerged 10 minutes in buffer before functionalization to dissolve the sucrose layer. Then the sensors were dipped for 15 minutes in 100 nM DNA containing solutions (biotinylated systems A-B) and rinsed in buffer solution (10 mM HEPES pH 7.4, 50 mM NaCl, 100 mM KCl and 0.05% v/v surfactant P20) for 10 minutes. The functionalized sensors were next dipped in different ruthenium(II) complex solution at different concentrations for 2 minutes interspersed by a rinsing step in the buffer solution during 4 minutes. Reference sensors without DNA immobilization were used to subtract the non-specific adsorption on the SA layer. The sensorgrams were fitted using a heterogeneous model. The reported values are the means of representative independent experiments, and the errors provided are standard deviations from the mean. Each experiment was repeated at least two times.

Computational studies

The geometry of all complexes were optimized at the B3LYP/6-31 g* level using Gaussian 09 software.[16] Although the chirality of the complexes might play a role in the binding association, enantiomeric resolution is beyond the scope of the present study. Therefore, for ease of interpretation, the Λ enantiomers of the complexes were chosen for the computational studies. For the targets we used for the quadruplex, the crystal structure of parallel quadruplexes from human telomeric DNA (PDB entry: 1KF1) whereas we had to construct an hairpin sequence similar to the one used for BLI experiments. First, an available hairpin sequence (PDB entry 2VAH) was modified by removing the nitrogenous base of the nucleotides differing from the BLI hairpin sequence. The abasic structure was then completed using xleap from the AMBER 12 software package,[17] solvated in a TIP3P water box. Sodium cations were added until the global charge was neutral and long-range electrostatic interactions were computed using the particlemesh Ewald method with a cut-off value of 10 . After minimization and heating, an MD simulation was run at 300 K for 10 ns with the time step set at 1 fs. Among the different hairpin conformations obtained, with the thymine residues moving in and out of the hairpin's T-loop, an "open" structure was selected to account for any possible insertion of the complexes inside the loop.

For docking calculations , we used the AutoDock 4.0 software package.[13] A grid of 80*80*80 points with a spacing of 0.5 Å

between these points was used; non-polar hydrogen atoms were merged and Gasteiger–Huckel charges were added on both the ligand and the target. The parameters for the Ru atom were set at r=2.96 Å, q= +2.0 and the van der Waals well depth was 0.056 kcal.mol^{-1}. The docking calculations involved a genetic algorithm search generating 50 docked structures. A default protocol was applied, with an initial population of 150 randomly placed individuals, a maximum number of 2.5*10^5 energy evaluations, a maximum number of 2.7*10^4 generations, a mutation rate of 0.02, and a crossover rate of 0.8. Results differing by less than 2 in positional root-mean square deviation (RMSD) were clustered together**.**

For the two docked positions of complex 1 against the quadruplex, NCI computations were performed using the NCI-Plot package[18] with the promolecular densities, using only the upper tetrad of 1KF1. For this analysis, since no parameter exists for the ruthenium atom, an iron atom was used.

Acknowledgements: M. G., G.P., M.D., M.A. and B. E. gratefully acknowledge the Université catholique de Louvain (UCLouvain), and the Prix Pierre et Colette Bauchau for financial support. This work was supported by the Fonds de la Recherche Scientifique (F.R.S.-FNRS) under grant no. U.N021.21 (B.E.) and the Collaborateur Scientifique fellowship (L.T.-G). This work was partially supported by the "Agence National de la Recherche": LabEx ARCANE and CBH-EUR-GS (ANR-17-EURE-0003), and the région Auvergne-Rhône-Alpes. The NanoBio-ICMG platforms (UAR 2607) are acknowledged for their support

Keywords: G-quadruplex DNA • Ruthenium complexes • Photo-oxidation• Doking experiments • Bio-layer interferometry

References[1]

[1] a) K. Lin, Z.-Z. Zhao, H.-B. Bo, X.-J. Hao and J.-Q. Wang, *Front. Pharmacol.* **2018**, *9*; b) J. Li and T. Chen, *Coord. Chem. Rev.* **2020**, *418*, 213355; c) S. A. McFarland, A. Mandel, R. Dumoulin-White and G. Gasser, *Curr. Opin. Chem. Biol.* **2020**, *56*, 23-27; d) J. Karges, S. Kuang, F. Maschietto, O. Blacque, I. Ciofini, H. Chao and G. Gasser, *Nat. Commun.* **2020**, *11*, 3262; e) K. Pobłocki, J. Drzeżdżon, T. Kostrzewa and D. Jacewicz, *Int. J. Mol. Sci.* **2021**, *22*, 8052; f) J. Karges, S. Kuang, Y. C. Ong, H. Chao and G. Gasser, *Chem. Eur. J.* **2021**, *27*, 362-370.

[2] A. E. Friedman, J. C. Chambron, J. P. Sauvage, N. J. Turro and J. K. Barton, *J. Am. Chem. Soc.* **1990**, *112*, 4960-4962.

[3] a) A. B. Tossi and J. M. Kelly, *Photochemistry and Photobiology* **1989**, *49*, 545-556; b) I. Ortmans, B. Elias, J. M. Kelly, C. Moucheron and A. Kirsch-DeMesmaeker, *Dalton Trans.* **2004**, 668-676; c) B. Elias and A. Kirsch-De Mesmaeker, *Coord. Chem. Rev.* **2006**, *250*, 1627-1641; d) S. Perrier, E. Mugeniwabagara, A. Kirsch-De Mesmaeker, P. J. Hore and M. Luhmer, *J. Am. Chem. Soc.* **2009**, *131*, 12458-12465.

[4] a) R. Bevernaegie, L. Marcélis, B. Laramée-Milette, J. De Winter, K. Robeyns, P. Gerbaux, G. S. Hanan and B. Elias, *Inorg. Chem.* **2018**, *57*, 1356-1367; b) R. Bevernaegie, B. Doix, E. Bastien, A. Diman, A. Decottignies, O. Feron and B. Elias, *J. Am. Chem. Soc.* **2019**, *141*, 18486-18491; c) J. Weynand, H. Bonnet, F. Loiseau, J.-L. Ravanat, J. Dejeu, E. Defrancq and B. Elias, *Chem-Eur. J.* **2019**, *25*, 12730-12739; d) J. Weynand, A. Moreno-Betancourt, F. Loiseau, N. Berthet, E. Defrancq and B. Elias, *Inorganic Chemistry* **2020**, *59*, 2426-2433.

[5] a) A. Granzhan, N. Kotera and M.-P. Teulade-Fichou, *Chem. Soc. Rev.* **2014**, *43*, 3630-3665; b) J. K. Barton, A. N. Boynton and K. M. Boyle in *Chapter 14 Targeting DNA Mismatches with Coordination Complexes*, The Royal Society of Chemistry, **2018**, pp. 367-390; c) K. Kawauchi, R. Urano, N. Kinoshita, S. Kuwamoto, T. Torii, Y. Hashimoto, S. Taniguchi, M. Tsuruta and D. Miyoshi, *Genes* **2020**, *11*, 1340; d) V. Sanchez-Martin, M. Soriano and J. A. Garcia-Salcedo, *Cancers (Basel)* **2021**, *13*, 3156; e) T. Rundstadler, E. Mothes, S. Amrane, J.-L. Stigliani, P. Verhaeghe and G. Pratviel, *J. Inorg. Biochem.* **2021**, *223*, 111551.

[6] a) Q. Deraedt, L. Marcelis, F. Loiseau and B. Elias, *Inorg. Chem. Front.* **2017**, *4*, 91-103; b) J. Weynand, A. Diman, M. Abraham, L. Marcélis, H. Jamet, A. Decottignies, J. Dejeu, E. Defrancq and B. Elias, *Chem. Eur. J.* **2018**, *24*, 19216-19227; c) M. Gillard, B. Laramée-Milette, Q. Deraedt, G. S. Hanan, F. Loiseau, J. Dejeu, E. Defrancq, B. Elias and L. Marcélis, *Inorg. Chem. Front.* **2019**, *6*, 2260-2270; d) M. Gillard, J. Weynand, H. Bonnet, F. Loiseau, A. Decottignies, J. Dejeu, E. Defrancq and B. Elias, *Chem. Eur. J.* **2020**, *26*, 13849-13860; e) T. Kench and R. Vilar in *Chapter Fourteen - Metal complexes as G-quadruplex binders*, *Vol. 54* (Ed. S. Neidle), Academic Press, **2020**, pp. 485-515.

[7] a) S. Neidle, *Nature Reviews Chemistry* **2017**, *1*, 0041; b) R. Hänsel-Hertsch, M. Di Antonio and S. Balasubramanian, *Nature Reviews Molecular Cell Biology* **2017**, *18*, 279-284; c) S. Asamitsu, N. Shioda and H. Sugiyama in *Chapter Three - Telomeric quadruplexes as therapeutic targets*, *Vol. 54* (Ed. S. Neidle), Academic Press, **2020**, pp. 77-99; d) N. Kosiol, S. Juranek, P. Brossart, A. Heine and K. Paeschke, *Mol. Cancer* **2021**, *20*, 40.

[8] G. Piraux, L. Bar, M. Abraham, T. Lavergne, H. Jamet, J. Dejeu, L. Marcélis, E. Defrancq and B. Elias, *Chem. Eur. J.* **2017**, *23*, 11872-11880.

[9] R. Bevernaegie, S. A. M. Wehlin, E. J. Piechota, M. Abraham, C. Philouze, G. J. Meyer, B. Elias and L. Troian-Gautier, *J. Am. Chem. Soc.* **2020**, *142*, 2732-2737.

[10] A. Kirsch-De Mesmaeker, R. Nasielski-Hinkens, D. Maetens, D. Pauwels and J. Nasielski, *Inorganic Chemistry* **1984**, *23*, 377-379.

[11] S. Steenken and S. V. Jovanovic, *J. Am. Chem. Soc.* **1997**, *119*, 617-618.

[12] A. Srishailam, Y. P. Kumar, P. Venkat Reddy, N. Nambigari, U. Vuruputuri, S. S. Singh and S. Satyanarayana, *J. Photochem. Photobiol. B: Biol.* **2014**, *132*, 111-123.

[13] G. M. Morris, D. S. Goodsell, R. S. Halliday, R. Huey, W. E. Hart, R. K. Belew and A. J. Olson, *J. Comput. Chem.* **1998**, *19*, 1639-1662.

[14] A. M. Brouwer, *Pure and Applied Chemistry* **2011**, *83*, 2213-2228.

[15] M. Wodon, S. De Kreijger, R. N. Sampaio, B. Elias and L. Troian-Gautier, *Photochem. Photobio. Sci.* **2022**.

[16] M. J. Frisch, G. W. Trucks, H. B. Schlegel, G. E. Scuseria, M. A. Robb, J. R. Cheeseman, G. Scalmani, V. Barone, G. A. Petersson, H. Nakatsuji, X. Li, M. Caricato, A. V. Marenich, J. Bloino, B. G. Janesko, R. Gomperts, B. Mennucci, H. P. Hratchian, J. V. Ortiz, A. F. Izmaylov, J. L. Sonnenberg, Williams, F. Ding, F. Lipparini, F. Egidi, J. Goings, B. Peng, A. Petrone, T. Henderson, D. Ranasinghe, V. G. Zakrzewski, J. Gao, N. Rega, G. Zheng, W. Liang, M. Hada, M. Ehara, K. Toyota, R. Fukuda, J. Hasegawa, M. Ishida, T. Nakajima, Y. Honda, O. Kitao, H. Nakai, T. Vreven, K. Throssell, J. A. Montgomery Jr., J. E. Peralta, F. Ogliaro, M. J. Bearpark, J. J. Heyd, E. N. Brothers, K. N. Kudin, V. N. Staroverov, T. A. Keith, R. Kobayashi, J. Normand, K. Raghavachari, A. P. Rendell, J. C. Burant, S. S. Iyengar, J. Tomasi, M. Cossi, J. M. Millam, M. Klene, C. Adamo, R. Cammi, J. W. Ochterski, R. L. Martin, K. Morokuma, O. Farkas, J. B. Foresman and D. J. Fox in *Gaussian 16 Rev. C.01*, *Vol.* Wallingford, CT, **2016**.

[17] D. Case, T. Darden, T. Cheatham, C. Simmerling, J. Wang, R. E. Duke, R. Luo, R. C. Walker, W. Zhang, K. Merz, B. Roberts, S. Hayik, A. Roitberg, G. Seabra, J. Swails, A. Götz, I. Kolossváry, K. F. Wong, F. Paesani and P. A. Kollman, *AMBER 12, University of California, San Francisco*, **2012**, p. 926-935.

[18] J. Contreras-García, E. R. Johnson, S. Keinan, R. Chaudret, J. P. Piquemal, D. N. Beratan and W. Yang, *J. Chem. Theory Comput.* **2011**, *7*, 625-632.

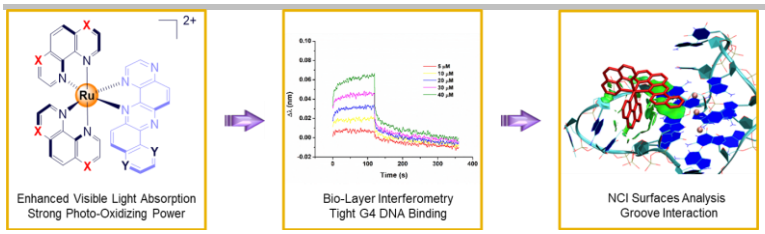

New Ru(II) complexes that gather strong photo-oxidizing power and enhanced visible light absorption were prepared with the highly conjugated dph or bpph ligands. Bio-Layer interferometry and NCI Surface analyses show their avid binding to G-quadruplex DNA particularly arising from interaction within the G-quadruplex groove.